Received: 30 May 2022 | Revised: 1 December 2023 | Accepted: 8 December 2023

DOI: 10.1111/ejn.16240

SPECIAL ISSUE ARTICLE

EJN European Journal of Neuroscience FENS WILEY

Temporal association between sleep spindles and ripples in the human anterior and mediodorsal thalamus

Orsolya Szalárdy[1,2] | **Péter Simor**[3,4] | **Péter Przemyslaw Ujma**[1] | **Zsófia Jordán**[5] | **László Halász**[5] | **Loránd Erőss**[5] | **Dániel Fabó**[5] | **Róbert Bódizs**[1]

[1]Institute of Behavioural Sciences, Semmelweis University, Budapest, Hungary

[2]Institute of Cognitive Neuroscience and Psychology, Budapest, Hungary

[3]Institute of Psychology, ELTE, Eötvös Loránd University, Budapest, Hungary

[4]UR2NF, Neuropsychology and Functional Neuroimaging Research Unit at CRCN, Center for Research in Cognition and Neurosciences and UNI-ULB Neurosciences Institute, Université Libre de Bruxelles, Brussels, Belgium

[5]National Institute of Mental Health, Neurology and Neurosurgery, Budapest, Hungary

Correspondence
Orsolya Szalárdy, Institute of Behavioural Sciences, Semmelweis University, Budapest 1089, Hungary.
Email: szalardy.orsolya@med.semmelweis-univ.hu

Funding information
ELTE Thematic Excellence Program 2020, Grant/Award Number: TKP2020-IKA-05; Ministry of Innovation and Technology of Hungary from theNational Research, Development and Innovation Fund, Grant/Award Number: TKP2021-EGA-25; National Research, Development and Innovation Office of Hungary Grant, Grant/Award Numbers: NKFI_FK_128100, K_128117

Edited by: Genevieve Albouy

Abstract

Sleep spindles are major oscillatory components of Non-Rapid Eye Movement (NREM) sleep, reflecting hyperpolarization-rebound sequences of thalamocortical neurons. Reports suggest a link between sleep spindles and several forms of high-frequency oscillations which are considered as expressions of pathological off-line neural plasticity in the central nervous system. Here we investigated the relationship between thalamic sleep spindles and ripples in the anterior and mediodorsal nuclei (ANT and MD) of epilepsy patients. Whole-night LFP from the ANT and MD were co-registered with scalp EEG/polysomnography by using externalized leads in 15 epilepsy patients undergoing a Deep Brain Stimulation protocol. Slow (~12 Hz) and fast (~14 Hz) sleep spindles were present in the human ANT and MD and roughly, 20% of them were associated with ripples. Ripple-associated thalamic sleep spindles were characterized by longer duration and exceeded pure spindles in terms of spindle power as indicated by time-frequency analysis. Furthermore, ripple amplitude was modulated by the phase of sleep spindles within both

Abbreviations: AASM, American Academy of Sleep Medicine; ANT, Anterior thalamic nucleus; CT, Computed tomography; DBS, Deep brain stimulation; EEG, Electroencephalogram; EMG, Electromyogram; FIR, Finite impulse response; IAM, Individual adjustment method; IEDs, Interictal epileptic discharges; IQ, General intelligence; LFP, Local field potential; M, Mean; MD, Mediodorsal thalamic nucleus; MI, Modulation index; mPFC, Medial prefrontal cortex; MRI, Magnetic Resonance Imaging; NREM, Non-rapid eye movement sleep; Ripple (NREM), Density of ripples during NREM sleep calculated as ripple number/minute of NREM; Ripple (sp), Density of ripples during sleep spindles calculated as ripple number/minute of spindles; SD, Standard deviation; SP (pure), pure sleep spindle; SP (ripple), ripple-associated sleep spindle; WAIS, Wechsler Adult Intelligence Scale.

thalamic nuclei. No signs of pathological processes were correlated with measures of ripple and spindle association, furthermore, the density of ripple-associated sleep spindles in the ANT showed a positive correlation with verbal comprehension. Our findings indicate the involvement of the human thalamus in coalescent spindle-ripple oscillations of NREM sleep.

Significance Statement

Thalamo-cortical loops are associated with sensory processing, memory formation and executive functions, many of which are tightly related to sleep state-dependent neural oscillations, such as sleep spindles. It was proposed that sleep-related epileptic transformation of normal neurological networks interferes with sleep-related synaptic homeostasis, neural plasticity and cognitive functioning. We had a unique opportunity to investigate the association between thalamic sleep spindles and ripples, and their associations with intellectual ability within two higher-order thalamic nuclei in human subjects, the anterior thalamic and mediodorsal thalamic nuclei. Our findings indicate the involvement of the human thalamus in sleep-spindle-related activity.

KEYWORDS

anterior thalamus, epilepsy, general intelligence, mediodorsal thalamus, sleep spindle, thalamic ripples

1 | INTRODUCTION

Higher-order brain functions rely on distributed networks involving the cortex and subcortical regions. The thalamus plays a crucial role in the proper functioning of these networks: thalamo-cortical loops are associated with sensory processing, memory formation and executive functions, many of which are tightly related to sleep state-dependent neural oscillations (Fama & Sullivan, 2015; Wolff et al., 2021). The thalamus also plays an important role in the coordinated connection between the cortex and hippocampus (Latchoumane et al., 2017). The human anterior thalamic nucleus (ANT) is a higher-order thalamic nucleus which is interconnected with the hippocampus (Aggleton et al., 2010). It has reciprocal connections with the anterior cingulate cortex, retrosplenial cortex and subiculum, and selective inactivation of the ANT leads to impaired memory formation similar to hippocampal lesions. Furthermore, the ANT plays an important role in the propagation of epileptic seizures and therefore became an important target for deep brain stimulation (DBS) which serves as a treatment for medically refractory epilepsy (Salanova, 2018). Another important higher-order nucleus in the human thalamus is the mediodorsal nucleus (MD) which is reciprocally connected with the medial prefrontal cortex (mPFC) and also receives inputs from parahippocampal regions, therefore it is assumed to interact with the cortex and hippocampus in declarative memory formation during non-REM (NREM) sleep (Mitchell & Chakraborty, 2013). Reduced MD volume was associated with decreased sleep spindle density in frontal brain regions, which suggests that the MD is involved in sleep spindle generation and/or propagation (Buchmann et al., 2014).

Sleep spindles are NREM sleep state-specific oscillations characterized by waxing/waning 10–16 Hz waveforms that are generated by the reticular nucleus of the thalamus and are propagated to other brain regions by thalamo-cortical circuits (Huguenard & McCormick, 2007; Steriade, 2005). The ANT has a tight anatomical and functional connection with the hippocampus, as well as different parts of the prefrontal cortex, and might act as an interface between them. Animal studies confirmed that dynamic reticular thalamic-thalamo-cortical interactions are responsible for the generation of sleep spindles (Steriade, 2005; Steriade et al., 1987), which were associated with cognitive functions such as learning and memory consolidation (Cairney et al., 2018; Saletin et al., 2011), and intellectual ability (Fogel & Smith, 2011; Ujma, 2018; Ujma et al., 2020). Several studies demonstrated that sleep spindles, and especially fast sleep spindles measured on the scalp have a close connection with cognitive performance and intelligence (Bódizs et al., 2005; Chatburn et al., 2013; Ujma, 2018), however, no data is available on the association between sleep spindles measured in the

human thalamus and intellectual ability. Furthermore, it has been demonstrated that epilepsy patients have altered sleep spindle function and structure, which is also related to the impairment of cognitive functions (Schiller et al., 2022).

Sleep spindles tend to co-occur with and coordinate the faster oscillations, called hippocampal ripples (~100–200 Hz), providing efficient off-line plasticity windows for memory consolidation and reorganization (Girardeau & Zugaro, 2011; Wilson & McNaughton, 1994). Besides neural plasticity sleep spindles were associated with pathological off-line plasticity in epileptic models and human epilepsy patients (Gelinas et al., 2016). Findings regarding the strong relationship between NREM sleep oscillations, neuroplasticity and epilepsy indicate that sleep-associated interictal epileptic discharges (IEDs) harm cognitive functions, inducing a significant cognitive loss (Halász et al., 2019).

The aim of the current study was to assess the function of ANT and MD in sleep-related neural oscillations measured by the association between thalamic sleep spindles and thalamic ripples during NREM sleep. It was proposed that sleep-related epileptic transformation of normal neurological networks, involving the hippocampus, thalamus and cortex, interfere with sleep-related synaptic homeostasis, neural plasticity and cognitive functioning (for a recent review, see Halász & Szűcs, 2020). In this pathway, the role of the human ANT and MD is not clear. Although different aspects of sleep spindle-related dynamic thalamocortical interactions were revealed (Mak-Mccully et al., 2017; Tsai et al., 2010), relationships between sleep spindles and ripples in the thalamus remained questionable. A recent report (Rektor et al., 2016) indicated the occurrence of high-frequency oscillations such as ripples in the human thalamus, however, results confirming the involvement of ripples in the thalamus are remarkably sparse. Furthermore, IEDs in the human thalamus, such as in the ANT LFP records were observed and suggested the involvement of ANT in the propagation of epileptic activity and contribute to the epileptic network (Hodaie et al., 2002; Sweeney-Reed et al., 2016). Here we investigated the association between thalamic sleep spindles and ripples within two higher-order thalamic nuclei in human subjects, the ANT and the MD.

2 | MATERIALS AND METHODS

2.1 | Participants

Subjects were 15 pharmacoresistant, surgically non-treatable epilepsy patients ($M_{age} = 36.9$ years, range: 17–64; 7 females) participating in the ANT deep brain stimulation (DBS) protocol at the National Institute of Mental Health, Neurology and Neurosurgery, Budapest, Hungary. These participants were selected from a larger pool of 20 patients, based on the following criteria: at least one whole night of seizure- and stimulation-free record consisting of co-registered thalamic LFP and scalp-EEG/polygraphy had to be available in the patients included in the study. Clinical and demographic data are reported in Table 1. The research was approved by the ethical committee of the National Institute of Mental Health, Neurology and Neurosurgery. Patients signed informed consent for participating in the study.

3 | EXPERIMENTAL DESIGN AND STATISTICAL ANALYSIS

3.1 | Psychometric evaluation

The psychometric evaluations were performed by experienced neuropsychologists using the Wechsler Adult Intelligence Scales, 4th edition (WAIS-IV, Wechsler, 2008). Data from 11 (out of the total 15 patients) patients were recorded, who underwent neuropsychological testing in the context of their clinical routine presurgical assessment. No WAIS-IV was completed from the remaining four participants.

From the 15 subtests, 10 core subtests were completed by 11 patients, resulting in full-scale IQ (FSIQ), and 4 composite indices, Verbal Comprehension Index (VCI), Perceptual Reasoning Index (PRI), Working Memory Index (WMI) and Processing Speed Index (PSI). The FSIQ is commonly used to estimate the individual's intellectual ability, derived from the 10 core subtests, whereas the index scores (VCI, PRI, WMI, PSI) are indicative for revealing disturbances affecting different cognitive domains (WAIS-IV index scores are reported in Table 2).

3.2 | Procedure

A pair of quadripolar Medtronic DBS electrodes were bilaterally and stereotaxically inserted into the anterior part of the thalamus during general anaesthesia. Contact lengths of the electrode are 1.5 mm, whereas intercontact spacing is 0.5 mm. The electrode diameter is 1.27 mm. Besides frontal transventricular and extraventricular trajectories, the posterior parietal extraventricular approaches were used in accordance with the decisions of the clinical-neurosurgical team. In accordance with the clinical protocol patients underwent a 48-hour, post-surgical video-EEG monitoring with externalized

TABLE 1 Clinical and demographic data of the patients.

Patient	Sex	WAIS IQ	Age at onset of epilepsy	Years since epilepsy onset	Etiology	Epilepsy syndrome	(inter)ictal EEG dominance	Highest phase of epilepsy evaluation	Earlier surgical interventions	Seizures/month before DBS	Medication (daily dose in mg)
#1	Female	NaN	34	30	Postencephalitis/negative MRI	Bitemp.	NA	Phase II-FO	-	12–14	Lacosamide 400, lamotrigine 400, oxcarbamazepine 600
#2	Male	NaN	12	5	Unknown	Bitemp.	Right	Phase II-FO, strip	-	12	Carbamazepine CR 800, lamotrigine 300, clonazepam 0.5, clobasam 20, quetiapine 50
#3	Female	64	15	23	Left HS	Bitemp.	Left	Phase II-FO	-	4–5	Carbamazepine CR 700, clobazam 20, zonisamide 200
#4	Female	61	1	22	Susp. Right cingular FCD	Bifront.	Left	Phase I	-	1	Clobasam 30 mg, lacosamide 400 mg, lamotrigine 200 mg
#5	Female	70	2	38	Unknown	Multifocal fronto-temporal	Right	Phase II-strip	-	2–4	Zonisamide 300, lamotrigine 250
#6	Male	97	11	32	Bilateral HS	Bitemp.	Left	Phase-I	-	1–2	Lamotrigine 300 mg, lacosamide 300 mg, cenobamate 400 mg
#7	Female	NaN	18	18	Bilat. Parietal polymicrogyria, bilat. HS	Bitemp.	Right	Phase II-FO	VNS	14–20	Levetiracetam 3000, carbamazepine 1500, zonisamide 400
#8	Female	92	12	13	Bilateral HS	Bitemp.	NA	Phase II-FO	VNS	30	Levetiracetam 3000 mg, lamotrigine 400 mg
#9	Female	94	23	18	Uncertain HS with left dominance	Bitemp.	Left	Phase II-FO	-	2–3	Lacosamide 300, levetiracetam 1500
#10	Female	71	12	34	Assumed HS	Bitemp.	Left	Phase II-FO	Right temporal resection	2–4	Clobasam 20, oxcarbamazepine 600, lacosamide 400, topiramate 200

TABLE 1 (Continued)

Patient	Sex	WAIS IQ	Age at onset of epilepsy	Years since epilepsy onset	Etiology	Epilepsy syndrome	(inter)ictal EEG dominance	Highest phase of epilepsy evaluation	Earlier surgical interventions	Seizures/month before DBS	Medication (daily dose in mg)
#11	Male	73	27	12	Left HS, postencephalitis	Multifocal fronto-temporal	Left	Phase I.	-	4	Lamotrigine 400 mg, brivaracetam 100 mg
#12	Female	71	20	19	Bilat. Subependymal heterotopia & non-regular hippocampal anatomy, left closed lip schizencephaly	Bitemp.	Right	Phase I	-	6–7	Carbamazepine 1500, topiramate 100
#13	Male	94	17	25	Left temporal dysgenesis, peritrigonal heterotopy	Left fronto-temporal	Left	Phase I	Left temporal resectio 2x, left peritrigonal heterotopy resectio	4–5	Perampanel 10 mg, lacosamide 500 mg, gabapentin 1200 mg, alprazolam 1 mg
#14	Male	NaN	19	7	Bilat. PVNH	Bitemp.	Right	Phase I	-	2	Oxcarbamazepine 1800, levetiracetam 2000, topiramate 300, sulthiam 300
#15	Male	57	19	16	Postencephalitis/negative MRI	Left fronto-temporal	Left	Phase II-strip + grid	Left temporal resection, VNS	6–10	Clonazepam 2, lamotrigine 425, phenobarbital 100, risperidone 2.5

[1]bitemp – bitemporal; FO – foramen ovale electrodes; CR – controlled release; HS – hippocampal sclerosis; PVNH – periventricular nodular heterotopia; VNS – vagus nerve stimulation; DBS – deep brain stimulation; Phase I – video-EEG monitoring with scalp electrodes; Phase II –video-EEG with invasive electrodes.

TABLE 2 WAIS-IV full-scale IQ and index scores.

	WAIS-IV full-scale IQ (FSIQ)	Verbal comprehension index (VCI)	Perceptual reasoning index (PRI)	Working memory index (WMI)	Processing speed index (PSI)
#1	NaN	NaN	NaN	NaN	NaN
#2	NaN	NaN	NaN	NaN	NaN
#3	64	70	75	66	65
#4	61	61	67	66	74
#5	70	68	90	60	76
#6	97	100	104	95	89
#7	NaN	NaN	NaN	NaN	NaN
#8	92	80	92	92	117
#9	94	98	96	86	97
#10	71	72	84	63	81
#11	73	70	84	74	81
#12	71	81	75	69	76
#13	94	95	98	97	89
#14	NaN	NaN	NaN	NaN	NaN
#15	57	56	65	55	76

thalamic leads, that is thalamic LFP co-registered with scalp EEG/polygraphy. The first 48 hours were recorded without thalamic stimulation (DBS-off). One whole-night seizure-free record of the 48-hour DBS-off records was selected and analysed in the present study.

3.3 | Individual localization of thalamic contacts

Thalamic contacts were localized by using the procedure described below (see also Simor et al., 2021). In order to individually localize the thalamic contacts preoperative MRI and postoperative CT images were co-registered using tools available in the FMRIB Software Library (FSL, Oxford, FLIRT, linear registration, 6 degrees of freedom). Threshold was applied on the co-registered CT scans to achieve the desired level of density for proper identification of the lead, thus removing the surrounding brain tissue. Coordinates of the most distal point of the lead were identified and a more proximal point was selected along the line of the contacts to mathematically reconstruct the coordinates of the centre point of each contact using Euclidean distance in three-dimensional spaces. These points superimposed over the T1 MRI image provided a guideline for contact localization by examining their location to the anatomical boundaries of the ANT. Anatomical positions according to standard coordinates of the contacts were double-checked by using the mamillothalamic tract as an anatomical guide to localize the ANT. In case of convergent results of these two methods, the ANT (for 15 patients) and MD (for 10 patients) data from contacts inside these nuclei were considered for further data analysis in the present study, data recorded from contacts outside the ANT and MD were excluded.

3.4 | Electrophysiological data recording a preprocessing

ANT and MD LFP, and all-night sleep EEG signals were recorded by SD-LTM 64 Express EEG/polygraphic recording system. Physiological signals were recorded at 8192 Hz/channel effective sampling rate with 22-bit precision and hardware input filters set at 0.02 (high pass: 40 dB/decade) and 450 Hz (low pass: 40 dB/decade). Data was decimated by a factor of 4 by the firmware resulting in stored time series digitized at 2048 Hz/channel. LFP signals were assessed by bilateral (L – left, R – right) quadripolar electrodes applying bipolar reference scheme and focusing only on those leads which were derived from two adjacent contacts positioned in the same thalamic nucleus or alternatively from the BRIDGE area (bipolar recordings with one contact within the ANT and the second contact in adjacent tissue Deutschová et al., 2021). The number of ANT and MD derivations recorded for each patient is reported in Table 3. Scalp

TABLE 3 Number of ANT and MD derivations for each patient.

Patient	Total number of ANT derivations	Left ANT derivations	Right ANT derivations	Total number of MD derivations	Left MD derivations	Right MD derivations
#1	**1**	0	1	**1**	0	1
#2	**2**	0	2	**1**	0	1
#3	**2**	0	2	**1**	0	1
#4	**3**	2	1	**0**	0	0
#5	**1**	1	0	**1**	1	0
#6	**4**	2	2	**0**	0	0
#7	**1**	0	1	**2**	0	2
#8	**6**	3	3	**0**	0	0
#9	**3**	1	2	**1**	0	1
#10	**3**	2	1	**2**	1	1
#11	**3**	2	1	**0**	0	0
#12	**2**	1	1	**2**	1	1
#13	**2**	1	1	**1**	1	0
#14	**4**	2	2	**0**	0	0
#15	**1**	0	1	**1**	0	1

EEG was recorded according to the international 10–20 system (Fp1, Fp2, Fpz, F3, F4, F7, F8, C3, C4, T3, T4, T5, T6, P3, P4, O1, O2, Oz; Jasper, 1958) extended with the inferior temporal chain (F9, F10, T9, T10, P9, P10) and two anterior zygomatic electrodes (ZA1, ZA2; Manzano et al., 1986), with the reference placed at the CP1 and ground placed at CP2 locations. Submental electromyograms (EMGs) were recorded by bipolarly referenced electrodes placed on the chin. For two patients (#1 and #2) the EEG electrode set was slightly different from the above-described montage. For patient #1 no Fpz, P9, P10 and EMG time series were recorded, and for patient #2 F3, F4, C3, C4, P3 and P4 electrodes were missing, although the electrode position at Pz was present in this patient. Data from missing electrodes were treated as missing values in further analyses.

Continuous EEG and LFP recordings were automatically segmented into 90-minute chunks by the recording software. During the recording session, there were no explicit light off and light on time, thus, the first and the last chunk for data analysis were selected as follows: a 90 minutes segment was required to contain at least 10 minutes of continuous sleep in the second or in the first halves, respectively for the first and last chunks. EEG data were offline re-referenced to the mathematically-linked T9 and T10 electrodes. All-night sleep records were scored for sleep-waking states and stages according to standard AASM criteria on 20 seconds basis (Berry et al., 2015) by an expert. Furthermore, artifactual segments were marked along the whole night record on 4 seconds basis and excluded from quantitative EEG and time series analyses. Artefacts were defined as muscle and movement artefacts, cardiac activity, large EEG deflections and not physiological signals that were analysed by a trained expert. Each 4 seconds window was rejected which contained any artifactual signal.

3.5 | Detection of IEDs and thalamic ripples

Data analyses were performed by MATLAB version 9.5 (R2018b, The MathWorks, Inc., Natick, MA; https://www.mathworks.com/products/new_products/release2018b.html) using the EEGlab toolbox 14.1.2b. For removing potential electric power-related noise, 4 Hz bandstop filter was applied centered at 50 Hz and its harmonics up to 400 Hz. For all data and frequency bands a zero-phase Hamming-windowed sinc finite impulse response (FIR) filter implemented in EEGlab (function pop_eegfiltnew contributed by A. Widmann) was used, which automatically calculates the transition bandwidth and filter order for the selected frequency bands. Ripple and IED detection was performed on the basis of the analysis method by Gelinas et al. (2016) within the NREM stages 2 and 3 sleep, separately for each contact. For removing potential epileptic activity (IEDs) continuous data of whole-

night ANT and MD LFP signals were band-pass filtered with a 25–80 Hz finite impulse response (FIR) filter. The filtered signal was then rectified (considering the absolute value of the signal) and normalized (*z*-score). IEDs were detected on the whole night NREM stages 2 and 3 sleep data (excluding artifactual data) as events where the filtered envelope (applying Hilbert transformation) exceeded two times the baseline (the mean of the filtered envelope on the whole night NREM stages 2 and 3 sleep data, excluding artefacts). Those events were then eliminated where the unfiltered signal envelope was two times below the baseline. Where two or more IEDs occurred within 1 s, only the one with the largest amplitude was kept. Spindles including any IEDs were rejected from the analysis (see below). For thalamic ripple detection, band-pass filtering of the whole-night ANT and MD LFP signals was performed at 100–200 Hz (FIR filter). The filtered signal was then rectified and normalized. Ripples were then detected as events where the filtered envelope exceeded 5 standard deviations of the baseline (the mean of the filtered envelope), and the mean envelope around the detected ripple event for a minimum of 20 ms and a maximum of 100 ms exceeded 2 standard deviations the baseline. The density of the ripples was calculated for the whole non-artifactual NREM sleep (in stage 2 and 3; (ripple number/minute of NREM defined as ripple (NREM) density) and separately for NREM sleep during the periods of sleep spindles (ripple number/minute of spindles i.e. the density of ripple events occurring during sleep spindle periods; defined as ripple (sp) density). Ripple (NREM) density (ripple number/minute of NREM sleep) and ripple (sp) density (ripple number/minute of sleep spindles) were compared by two-tailed Student's t-tests, to investigate whether ripples occur evenly during NREM sleep or occur more frequently during periods of sleep spindles, separately for the ANT and MD, using JASP 0.15.0.0.

3.6 | Sleep spindle detection and analysis

Non-artifactual NREM sleep EEG and thalamogram records were subjected to the Individual Adjustment Method (IAM) of sleep spindle analysis (Bódizs et al., 2009; Ujma et al., 2015). Frontally dominant slow and parietally dominant fast sleep spindles were defined for each patient and each EEG and thalamic channel using individual-specific frequency criteria, as well as associated individual- and derivation-specific amplitude criteria in the 9–16 Hz all-night NREM sleep. Detailed method of sleep spindles detection is reported by Bódizs et al. (2009) and Ujma et al. (2015). For short, individually adjusted frequency limits of slow and fast sleep spindles were determined by the second-order derivatives of the 9–16 Hz amplitude spectra (0.25 Hz resolution). Derivation-specific second-order derivatives of the amplitude spectra were averaged over all scalp EEG derivations, separately for each patient. Individual-specific frequency limits of sleep spindles are defined as pairs of zero crossing points encompassing a negative peak in the whole-scalp second-order derivatives. Thus, the zero crossing points define the individual frequency limits and ranges of sleep spindles, separately for the fast and slow spindles. Afterwards, derivation-specific amplitude criteria were calculated. The signal was then band-pass filtered for the individual slow and fast spindle frequency ranges. The filtered signal was then rectified and smoothed by a moving average weighted with a Hanning window of 0.1 s length and multiplied with $\pi/2$. Spindles were detected where the envelopes of the band-pass filtered and rectified data exceeded the individual and derivation-specific threshold as defined above for at least 0.5 s. Thalamic sleep spindles contaminated with assumed IEDs (see below) were removed from further analyses, as IEDs with increased activity in the spindle frequency range may be falsely detected as spindles. The remained sleep spindles were categorized based on their association with or without ripples. If one or more ripple was detected during the spindle, that spindle was categorized as ripple-associated spindle, SP (ripple). Spindles without any association with ripples were categorized as pure sleep spindles, SP (pure**).** The non-averaged number of sleep spindles (including the association of ripples and IEDs) for all thalamic contacts is reported here: https://osf.io/zcr3j. The spindle densities (spindle number/minute of NREM) were calculated separately for each category. Sleep spindle density data were averaged across appropriate derivations within a nucleus, separately for the ANT and MD, and for the fast and slow spindles. The duration of sleep spindles was measured as the time interval from spindle onset and offset, separately for each spindle category. Spindle duration data from all derivations corresponding to the same nucleus were averaged, separately for the ANT and MD, and for the fast and slow spindles. Averaged sleep spindle density and duration (including the association with or without ripples), and averaged ripple density (ripple number/minute of NREM or/minute of spindles) are reported here: https://osf.io/z9dsq.

Overall averaged sleep spindle density and duration for the patients were compared across nuclei performing repeated-measures ANOVA with the factors spindle type (slow vs. fast) × nucleus (ANT vs. MD), where missing values were handled as missing data. Comparison of SP (ripple/pure) density and duration were performed by repeated-measure ANOVA with the factors spindle type

(slow vs. fast) × association (ripple vs. pure) × nucleus (ANT vs. MD). Post-hoc tests were conducted by Tukey's HSD. Statistical analyses were performed by JASP 0.15.0.0.

Time-frequency wavelet analysis was performed on 4600 ms long epochs extracted in the −2300 to 2300 ms latency range around sleep spindle onsets (separately for the slow and fast SP (ripple/pure)) on all ANT and MD derivations. Time-frequency analysis was performed by Morlet wavelet transformation with linearly increasing cycle numbers from 4 cycles to 20 cycles for the 1–450 Hz frequency range using 0.5 Hz frequency resolution in the 1–40 Hz range, 1 Hz frequency resolution in the 41–80 Hz range and 5 Hz frequency resolution in the 81–450 Hz range. The baseline interval was set at −2000 ms to 0 ms before sleep spindle onset. Time-frequency power spectra were averaged across all derivations within the same nucleus, separately for the fast and slow SP (ripple/pure). We compared the time-frequency power values for the SP (ripple) with SP (pure) using a cluster-based permutation test (Maris & Oostenveld, 2007) in the window 0–1.5 s from spindle onset, on the frequency range of 1–450 Hz. For each nucleus (ANT and MD) and spindle (slow and fast), the permutation test was performed by computing 10,000 permutations using the *t*-statistic. The permutation threshold was set at $p < 0.025$. Cluster-based correction for multiple comparisons was applied with a cluster significance threshold of $p < 0.05$.

For assessing phase-amplitude coupling between sleep spindle phases and ripple amplitudes in the thalamus, the modulation index (MI) was calculated based on the method by Tort et al. (2010). As the use of a bipolar montage inherent to LFP recordings in small anatomical structures prevents the unequivocal determination of polarity (Clemens et al., 2011), MI were calculated separately for each patient and each thalamic derivation. First, 4600 ms long epochs were extracted around individual sleep spindles with co-occurring ripples (SP (ripple)), in the −2300 to 2300 ms latency range where 0 ms corresponds to the onset of sleep spindles. All detected SP (ripple) data were band-pass filtered in the frequency bands of interest, 80–200 Hz for extracting the ripple amplitude and individual slow and fast spindle bands, detected by the IAM of sleep spindle analysis (see above) for extracting instantaneous phase of sleep spindles (FIR filter). Bandpass-filtered data were then Hilbert transformed using the 0–2000 ms time range to avoid edge effects. MI was then calculated for each electrode using 18 phase bins from $-\pi$ to $+\pi$, pooling all phase and amplitude values extracted from the epoched data (all detected sleep spindles), separately for each patient, electrode and fast and slow spindles. The observed MI was then subjected to permutation testing in order to quantify the difference between the observed MI and the distribution of shuffled coupling values. Shuffled MI distribution was calculated by measuring the MI between the original phase time series and permuted amplitude time series where amplitude data points were randomly shuffled, using 1000 iterations, separately for each patient and electrode. The observed MI values were then z-standardized to the shuffled phase-amplitude coupling distribution, where normalized z-values directly reflect p-values, and MI(z) equal to 1.645 corresponds to the 5% p-value. Thus, MI(z) values larger than 1.645 reflect a significant spindle-ripple coupling in the thalamus. Bonferroni correction was applied for multiple comparisons.

We aimed to estimate the time dynamics of spindle co-occurrence between thalamic and cortical channels. Spindle co-occurrence was defined in the following way: when the initiation of a sleep spindle was detected on any channel (cortical or thalamic), all subsequent spindles initiating on any other channel before the end of the original spindle were considered to co-occur, comprising a single spindle event involving multiple channels with a time lag on each channel, defined as the time difference of spindle initiation relative to the first spindle. For thalamocortical co-occurrence analysis, we selected all instances when sleep spindles co-occurred on both 1) a selected scalp channel (F3 or F4 for frontal spindles, P3 or P4 for parietal spindles, for patient #2 Fp2-Fpz and Pz-Oz instead) and 2) on a channel localized in a specific thalamic nucleus (ANT or MD). That is, the analysis included spindles which could originate elsewhere but were later detected on both specific scalp channels and in the thalamus. We defined thalamocortical spindle lags as the time lag (relative to the first spindle) of the scalp channel minus the time lag of the thalamic channel. We modelled spindle lags with a linear mixed model implemented in the MATLAB 2017a fitlme() function using lag as the dependent variable, spindle type, thalamic nucleus and scalp channel as fixed effects with random intercepts by the patient (Ujma et al., 2022).

For assessing the potential correlates and functions of thalamic ripples and spindles Pearson correlations coefficient was calculated to explore the relationship between sleep spindle density (thalamic SP (ripple) and SP (pure) density) and clinical epilepsy characteristics (years since epilepsy onset and seizures/month [before DBS]), separately for the ANT and MD, and for the slow and fast spindles. Pearson correlation coefficients were also calculated for sleep spindle density and WAIS-IV FSIQ/index scores; separately for the ANT and MD, and for the slow and fast spindles. Correlation coefficients were calculated by STATISTICA 13.1. For multiple comparisons, Bonferroni correction was applied, with the aim of controlling

Type I error, separately for the analysis of WAIS-IV scores and clinical epilepsy characteristics.

4 | RESULTS

Sleep architecture is reported in Table 4 for each patient.

4.1 | Ripple density during sleep spindles and overall NREM sleep

Ripple (NREM) and ripple (sp) density were not significantly different from each other (Figure 1) neither in the ANT ($t_{14} = 1.427$, $p = 0.352$) nor in the MD ($t_9 = 2.293$, $p = 0.096$), after correction for multiple comparisons.

TABLE 4 Sleep architecture of the night records of the patients (all measures are reported in minutes).

Patient	Total recording time (min)	Sleep duration (min)	WASO (min)	Wake (min)	S1 (min)	S2 (min)	S3 (min)	REM (min)
#1	690.3	416	187	274.6	59.3	226.7	38.7	91.3
#2	596	542.3	29.6	53.7	45.3	312	66.7	118.3
#3	630	522	88.7	108	19	420.7	16.7	65.7
#4	540	401.3	106	138.7	40	300.7	31.3	29.3
#5	576.6	425.3	132.3	151.3	158.7	234.3	0	32.3
#6	540	373	165	167	67.3	293.3	0	12.3
#7	503	461.3	38.7	41.7	10	296.7	86	68.7
#8	450	397	29.3	53	24	168	82.7	122.3
#9	720	574.3	56.7	145.7	15.7	433.3	53.3	72
#10	630	493.3	119.3	136.7	25.7	386.3	36.3	45
#11	450	294.3	155.6	155.7	34	174.3	20	66
#12	455	333.7	41	121.7	34.7	150.7	118.7	29.7
#13	450	347.3	76.3	102.7	26.3	274.3	14.3	32.3
#14	600	560	30	40	47	295.7	98	119.3
#15	662.6	247.7	92.3	415	62	146.3	0	39.3
Mean	566.2333	425.92	89.85333	140.3667	44.6	274.22	44.18	62.92
(SD)	91.36567	98.80544	53.12365	97.21778	35.95128	92.39791	38.37701	36.11547

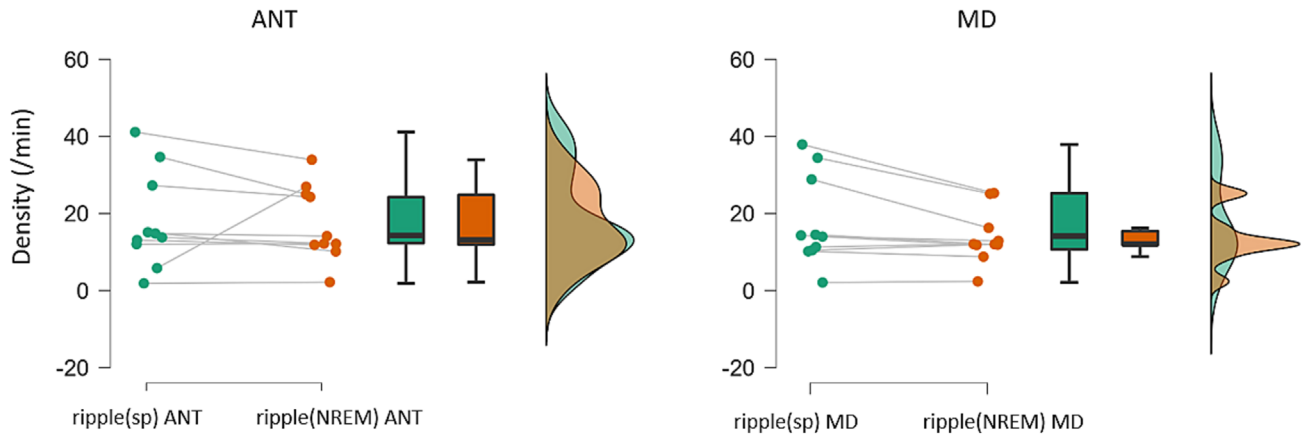

FIGURE 1 Ripple density in the ANT (left) and MD (right). Ripple (sp) reflects the ripple density during sleep spindles (ripple number/minute of spindles), ripple (NREM) reflects the density of ripples measured during the whole non-artifactual NREM sleep (ripple number/minute of NREM).

4.2 | Overall sleep spindle density and duration in the ANT and MD

For the overall sleep spindle density (Figure 2), the main effect of spindle type and nucleus was not significant (nucleus: $F_{1,9} = 3.432$, $p = 0.097$ spindle type: $F_{1,9} = 3.490$, $p = 0.095$), but there was a significant interaction between these factors ($F_{1,9} = 6.203$, $p = 0.034$). Post-hoc test revealed that the interaction was caused by the significantly lower fast spindle density in the MD compared to the ANT (p = 0.039). Main effect of spindle type was significant for the duration of sleep spindles ($F_{1,9} = 5.756$, $p = 0.040$) due to the longer slow sleep spindles compared to fast sleep spindles. Main effect of the nucleus was not significant ($F_{1,9} = 0.126$, $p = 0.730$) and no interaction occurred between these factors ($F_{1,9} = 2.621$, $p = 0.140$) on the duration of sleep spindles.

4.3 | Sleep spindle density and duration SP (pure/ripple) in the ANT and MD associated with and without ripples

Figure 3 shows examples of fast sleep spindles from the same patient and nucleus, associated with and without ripples. A significant main effect of association was found for the spindle density ($F_{1,9} = 53.180$, $p < 0.001$, $\eta p^2 = 0.855$), due to the higher SP (pure) density compared to the SP (ripple) density. The main effect of spindle type and nucleus was not significant (spindle type: $F_{1,9} = 3.489$, $p = 0.095$, $\eta p^2 = 0.279$; nucleus: $F_{1,9} = 3.432$, $p = 0.097$, $\eta p^2 = 0.276$), but again, significant interaction occurred between these factors ($F_{1,9} = 6.202$, $p = 0.034$, $\eta p^2 = 0.408$) caused by the lower fast sleep spindle density in the MD compared to the ANT (p = 0.027) as reported above at the overall sleep spindle density analysis. The duration of sleep spin-

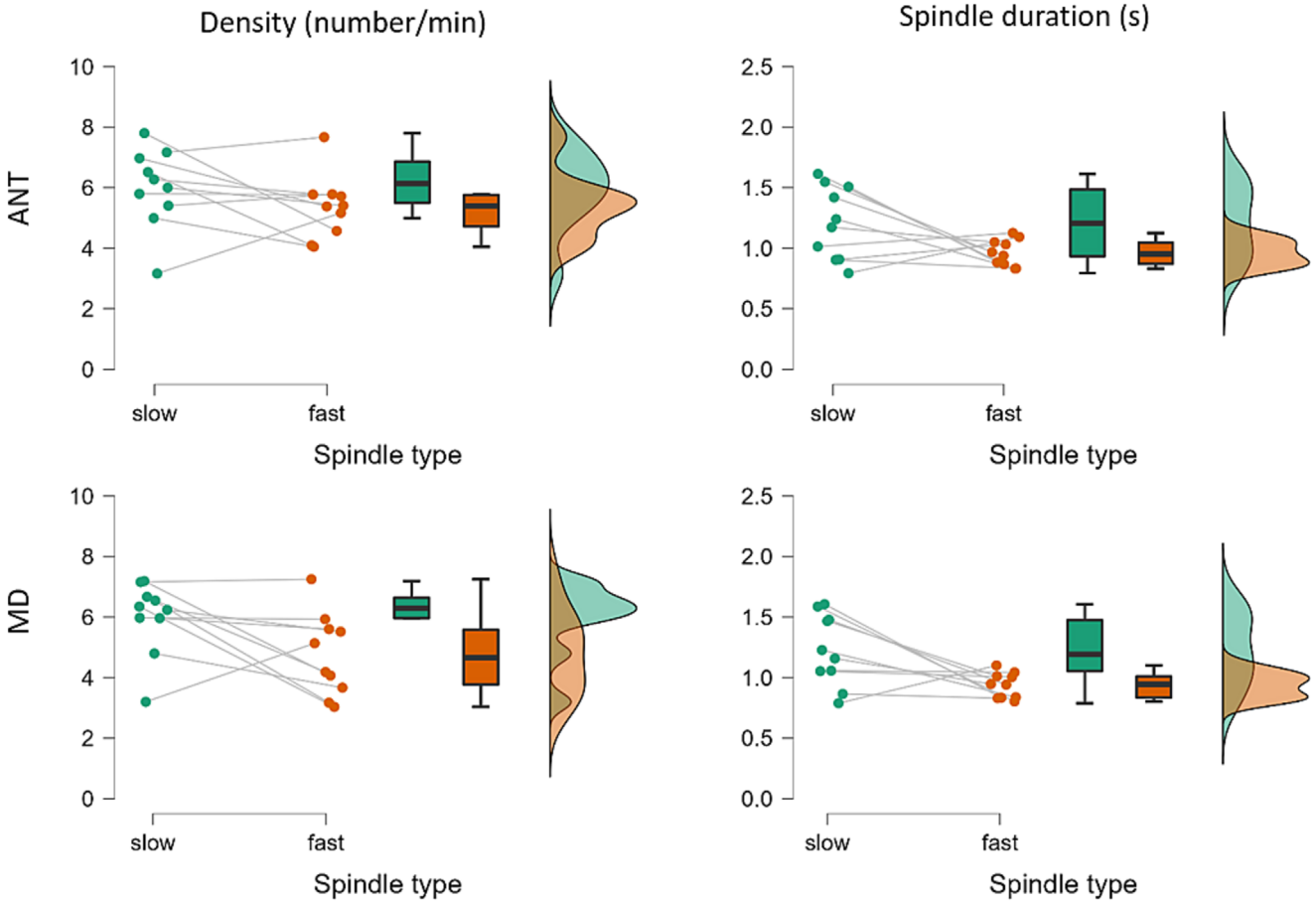

FIGURE 2 Overall sleep spindle density (left panel) and duration (right panel) in the ANT (top) and MD (bottom), separately for the slow spindles (green dots) and fast spindles (orange dots).

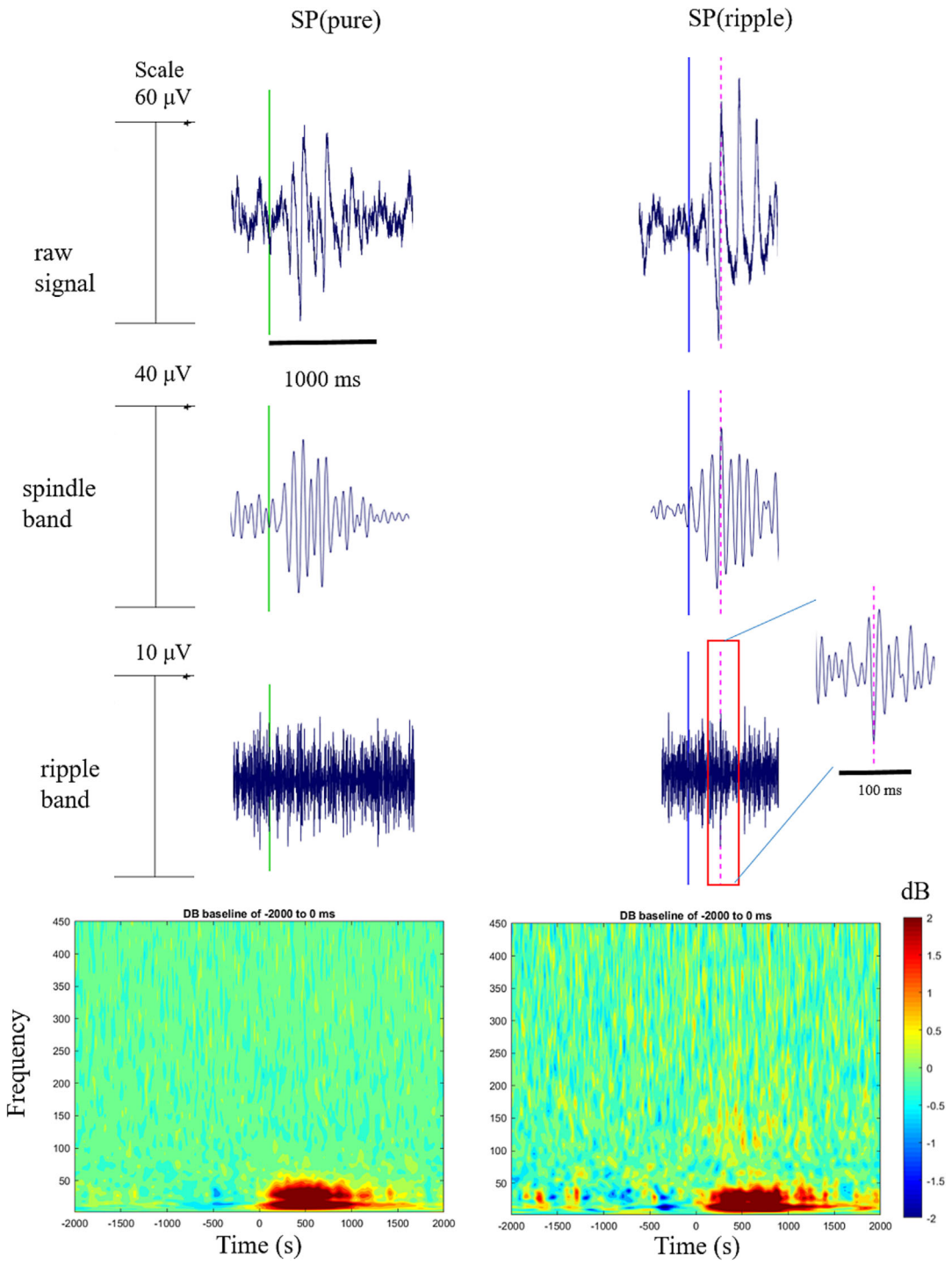

FIGURE 3 Examples of sleep spindles detected in the ANT from Patient #10: fast SP (pure) (left), and SP (ripple) (right). Upper row: 5 Hz highpass-filtered signal (raw signal), second row: 10–16 Hz bandpass-filtered signal (spindle band), third row: 100–200 Hz bandpass filtered signal (ripple band) of the same sleep spindle within each category. The fourth row depicts the time-frequency power spectra averaged across all fast sleep spindles of the same category detected in one ANT derivation of the same patient. The timepoint "0", and the green and blue lines indicate the onset of sleep spindles.

dles was affected by the ripple association, as indicated by the significant main effect of association ($F_{1,9} = 54.661$, $p < 0.001$, $\eta p^2 = 0.858$), on average, ripple-associated spindles were 232 ms longer than pure spindles (Figure 4). The main effect of spindle type was also significant, as longer slow spindles were detected

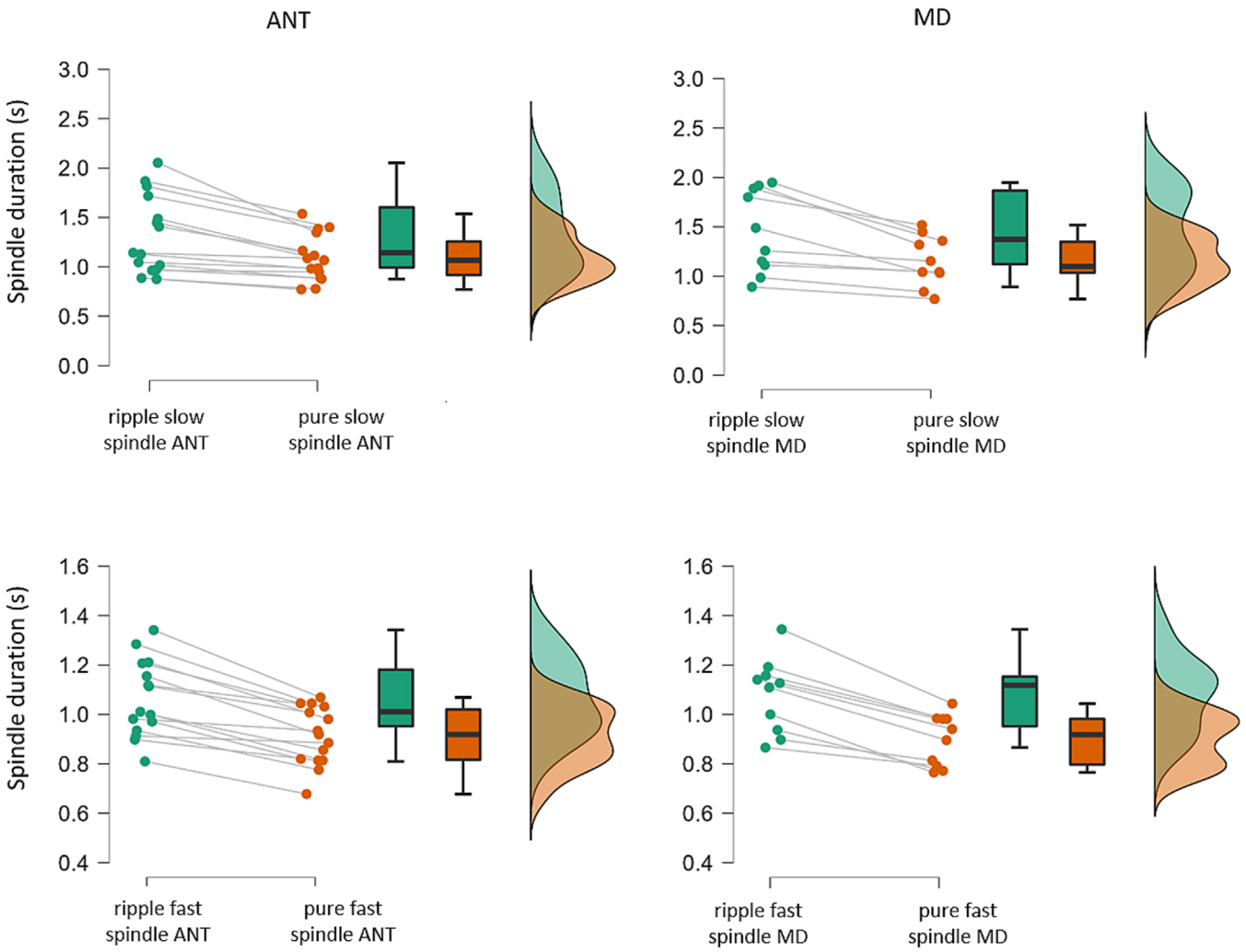

FIGURE 4 Sleep spindle duration in the ANT (left) and MD (right), separately for the ripple-associated and pure slow spindles (upper row) and fast spindles (bottom row). The green and orange dots represent the ripple-associated, and the pure sleep spindles, respectively.

compared to the fast spindles ($F_{1,9} = 5.577$, $p = 0.0425$, $\eta p^2 = 0.383$). The main effect of the nucleus was not significant ($F_{1,9} = 0.404$, $p = 0.541$, $\eta p^2 = 0.043$), and no interaction occurred between the factors ($p > 0.137$, at least).

4.4 | Power spectral density in the time-frequency domain of pure and ripple-associated spindles

The cluster-based permutation test revealed two significant clusters between SP (ripple) and SP (pure), both for the ANT and MD and for the fast and slow sleep spindles. In all cases, increased power was observed for SP (ripple) compared to SP (pure) (Figure 5). For the ANT fast spindles, a significant difference was detected in the time window of 0–940 ms and frequency window of 58–200 Hz ($p < 0.0001$) and in the time window of 760–1500 ms and frequency window of 12–36 Hz ($p = 0.0092$). Similar results were found for the ANT slow spindles, where the low-frequency difference was extended: significant difference was found in the time window of 0–1000 ms and frequency window of 50–200 Hz ($p < 0.0001$) and in the time window of 485–1360 ms and frequency window of 4.5–60 Hz ($p = 0.0023$). Significant clusters occurred in the MD in the 0–800 ms time and 80–200 Hz frequency window ($p = 0.0068$), as well as in the 590–1200 ms time and 8–45 Hz frequency window ($p = 0.0068$) for the fast spindles, and in the 0–1030 ms time and 75–250 Hz frequency window ($p = 0.0156$) and 680–1500 ms time and 8.5–25 Hz frequency window ($p = 0.0293$) for the slow spindles.

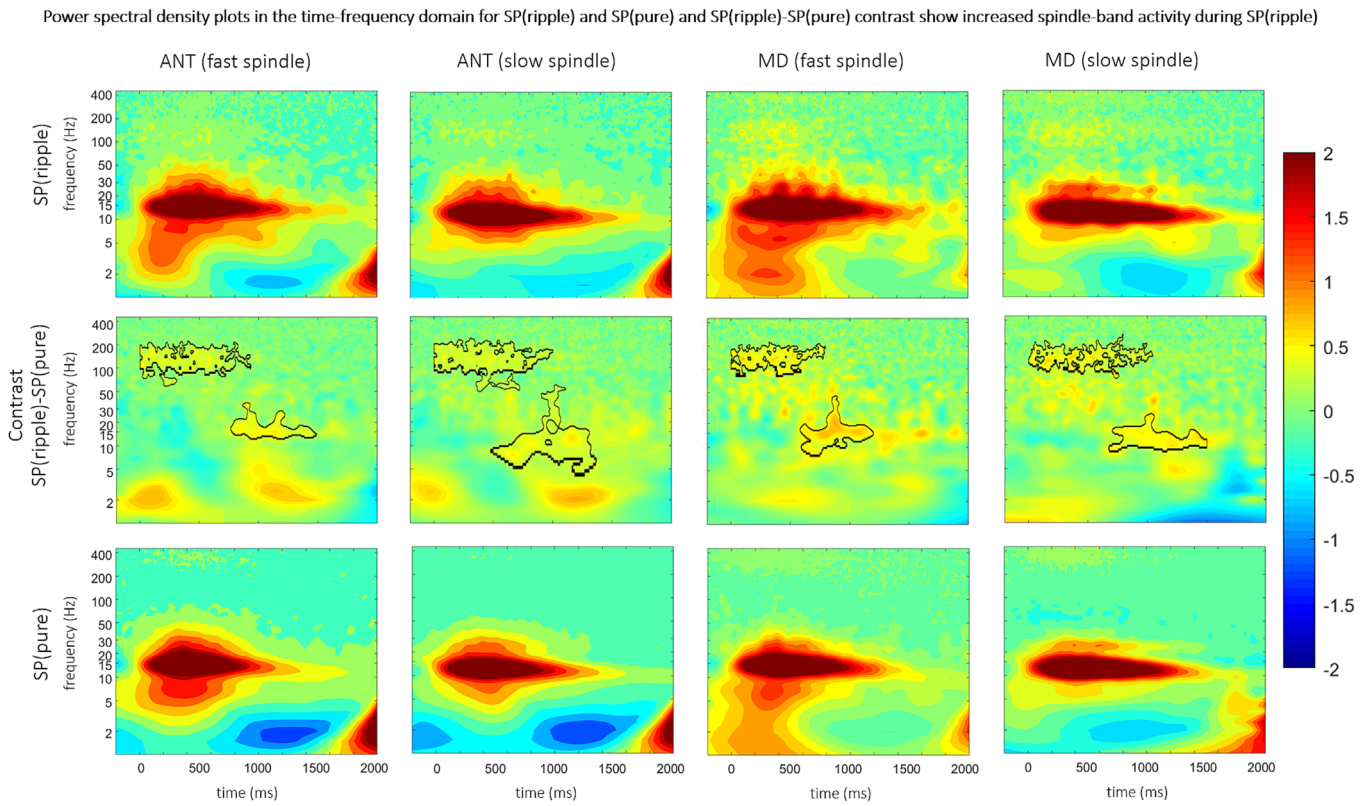

FIGURE 5 Power spectral density plots in the time-frequency domain for the slow and fast sleep spindles measured in the ANT and in the MD, separately for the SP (ripple) –top panels– and SP (pure) –bottom panels–, within the 1–450 Hz frequency range. The middle panels show the power spectral density differences between SP (ripple) and SP (pure). The timepoint "0" indicates the onset of sleep spindles. Significant differences indicated by the cluster-based permutation test ($p < 0.05$) are circumscribed by the black lines. All time-frequency maps were displayed from 2 to −2 dB, and frequency is represented in a logarithmic scale.

4.5 | Spindle-ripple coupling in the thalamus

For all but one electrode position, the permutation test revealed that the observed MI were significantly larger than the permuted MI (for Patient #8 ANT fast spindle $p = 0.0024$, for all other p's < 0.0001), both in the ANT and MD, separately for the slow and fast sleep spindles, except a single MI value for the slow sleep spindles in one ANT derivation for patient #2, where $p = 1.00$ applying Bonferroni correction (mean MI_Z ANT fast spindle: 22.56, $p < 0.0001$, *SD*: 19.00; mean MI_Z ANT slow spindle: 22.01, $p < 0.0001$, *SD*: 15.93; mean MI_Z MD fast spindle: 92.07, $p < 0.0001$, *SD*: 224.09; mean MI_Z MD slow spindle: 89.54, $p < 0.0001$, *SD*: 201.83). Figure 6 shows a representative example of the spindle phase and ripple coupling in the ANT. MI_Z and p values are reported in Supplementary Table S1, separately for each ANT and MD derivation.

4.6 | Spindle dynamics in the thalamus and the cortex

The distribution of thalamocortical lags (broken down by ripple co-occurrence) is shown in Figure 7. In short, thalamocortical lags were generally either negative or not significantly different from zero, indicating that either sleep spindles preferentially occurred on the scalp first or occurred simultaneously on the scalp and thalamic channels. Very little variance in spindle lag was accounted for by this model ($R2 = 0.014$), suggesting that lag mainly depends on extraneous factors. Still, fast spindles ($\beta = 0.015$), spindles in the MD nucleus ($\beta = 0.017$) and spindles occurring on F4 ($\beta = 0.010$) were associated with more positive lags, while spindles occurring on P3 ($\beta = -0.007$) and spindles with ripples ($\beta = -0.017$) were associated with more negative lags. That is, in the case of fast spindles, in the MD and on F4, there was a diminished tendency for scalp spindles to occur first, but this tendency increased on P3 and especially when ripple

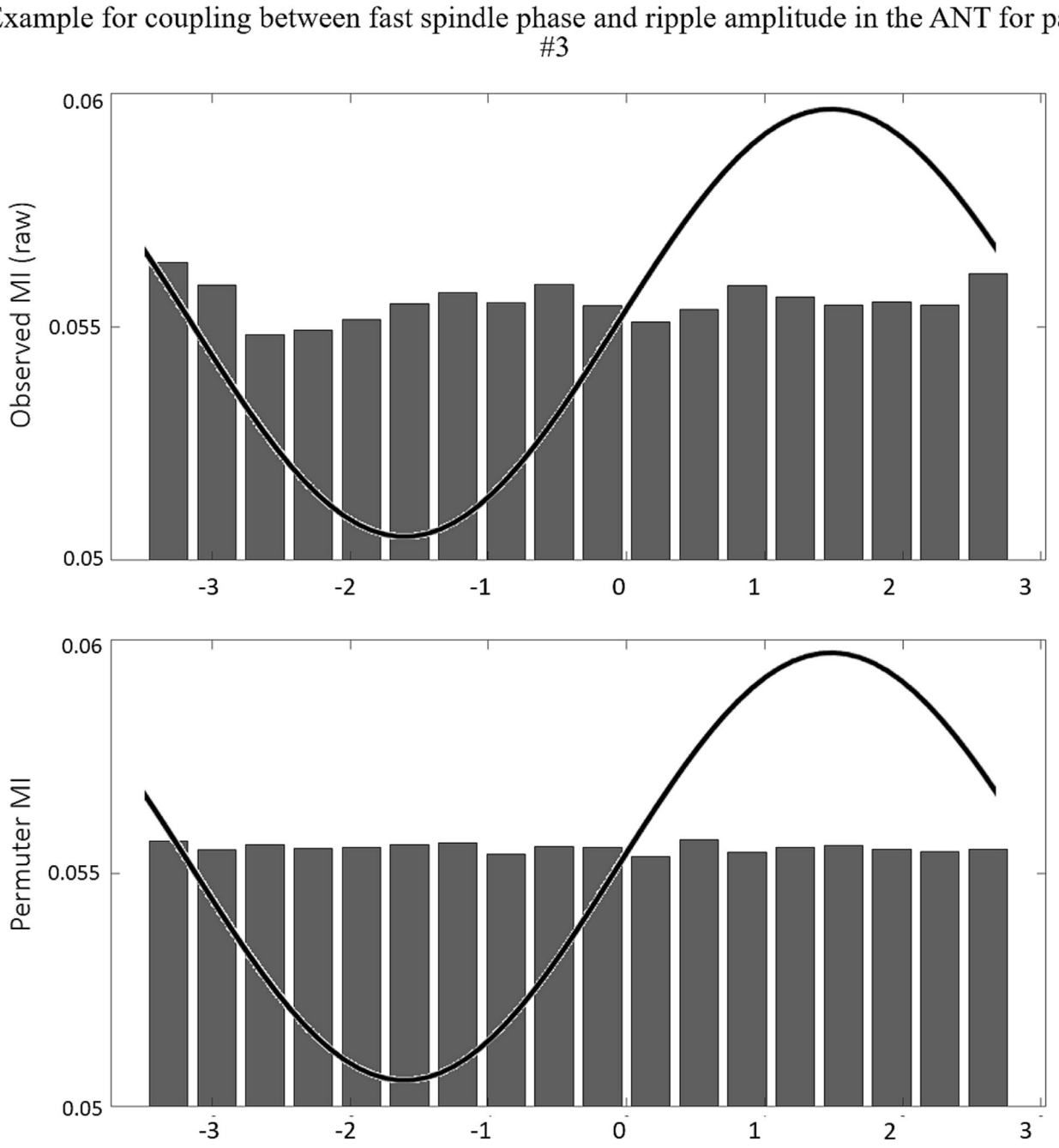

FIGURE 6 Example phase-amplitude coupling between fast spindle phase and ripple amplitude measured in the ANT for patient #3. MI(z) measured for this electrode position is 27.00, $p < 0.00001$. The sine wave represents one cycle of the sleep spindle.

activity was present in the thalamus. All effect sizes are unstandardized and given in seconds. All $p < 0.001$, except for the effect associated with P3 ($p = 0.010$).

4.7 | The relation between thalamic spindles, clinical epilepsy characteristics and WAIS-IV FSIQ and index scores

Forty correlations were calculated between WAIS-IV FSIQ and index scores and spindle density; thus, the Bonferroni-corrected p-value was 0.00125. Statistical analysis revealed that when thalamic sleep spindles were separated according to their associations with and without ripples, positive correlations were observed between VCI and ripple-associated fast spindle density in the ANT (Figure 8), which survived the Bonferroni correction ($r = 0.874$, $N = 11$, $p < 0.000$). There were no statistically significant correlations in other domains after the Bonferroni correction. For all comparisons, Supplementary Table S2 summarizes the Pearson correlation coefficient (r) and p values.

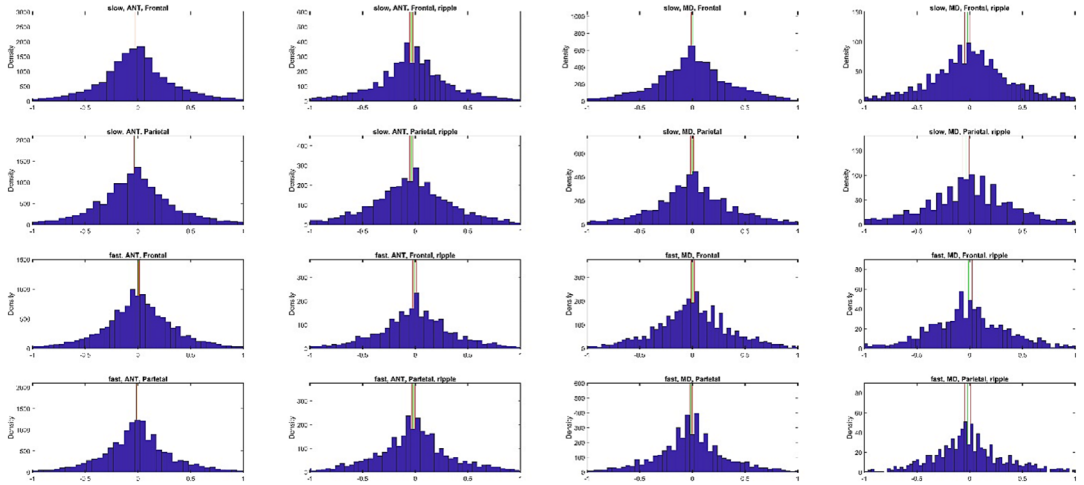

FIGURE 7 Thalamocortical spindle lags by ripple occurrence. Histograms show the time lag difference of scalp minus thalamic spindles by scalp region, thalamic nucleus, ripple presence and spindle type (slow or fast), pooled across all patients. Vertical green lines show the mean lag and red lines indicate the 95% CIs. Negative values indicate that spindles preferentially occur on the scalp first and vice versa. Axis X on each histogram is truncated at [−1 1] seconds for optimal visibility.

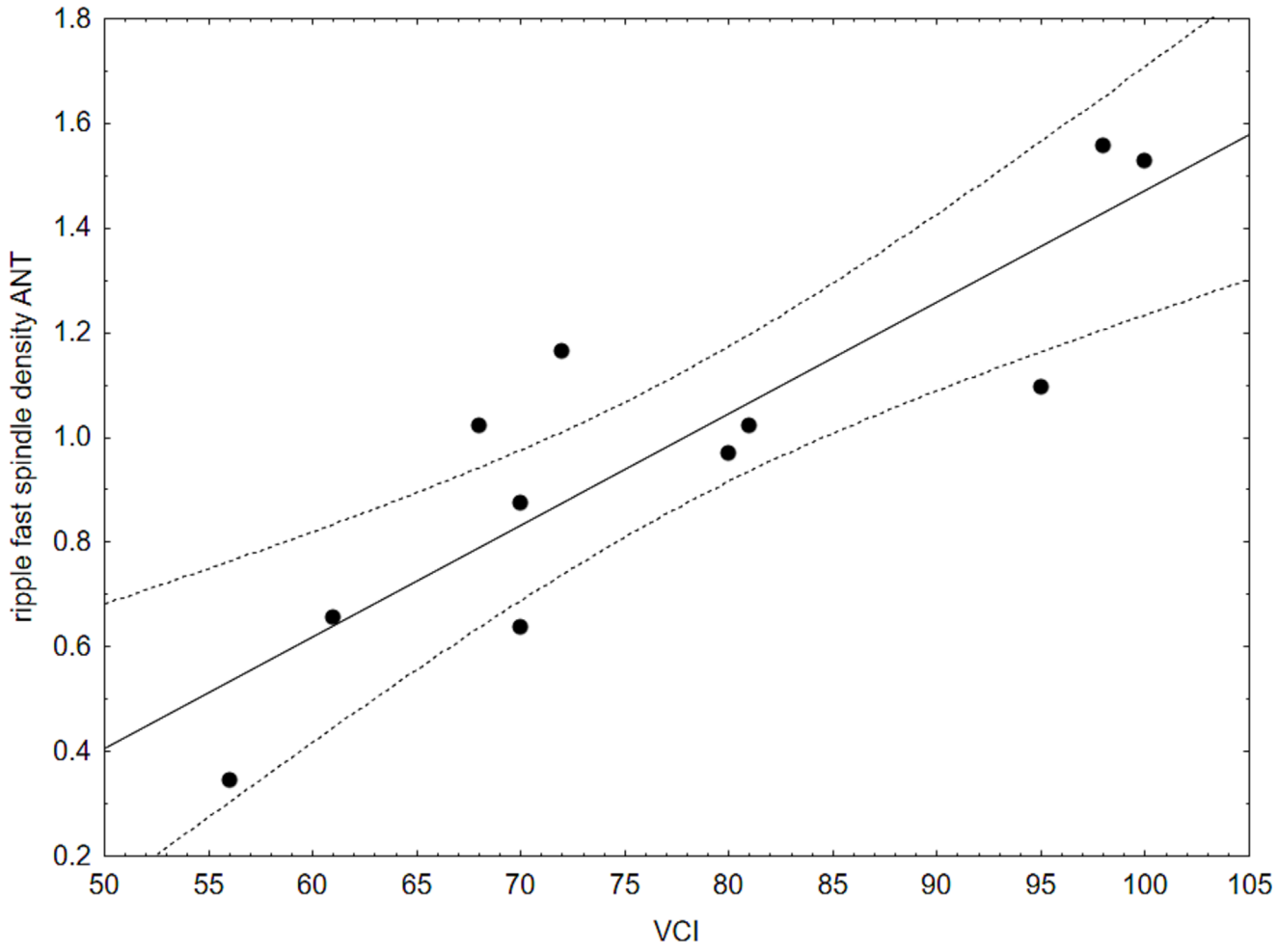

FIGURE 8 Correlation between ripple-associated fast sleep spindle density in the ANT and verbal comprehension index.

For assessing the relationship between sleep spindle density and clinical epilepsy characteristics, 16 correlations were calculated between years since epilepsy onset, seizure prevalence and spindle density; thus the Bonferroni corrected p-value was 0.003125. No significant correlation occurred between the ANT and MD spindle density (SP (pure) and SP (ripple)) and years since epilepsy onset ($p > 0.061$), and with seizure prevalence ($p > 0.05$). All results are reported in Supplementary Table S3.

5 | DISCUSSION

We investigated the occurrence of sleep spindles and ripples in the human anterior and mediodorsal thalamus. Sleep spindles were detected both in the ANT and MD. The occurrence of sleep spindles in the human ANT was confirmed in previous studies (Tsai et al., 2010). We demonstrated that spindles are also present in the human MD. The duration of slow and fast spindles was similar in the two thalamic nuclei; however, the overall density of fast sleep spindles was lower in the MD compared to the ANT. In the majority of cases where thalamic-scalp sleep spindle co-occurrences were detected, ANT and MD sleep spindles slightly lagged behind cortical ones, which coheres with available reports (Tsai et al., 2010) and suggests the prevailing role of corticofugal fibres in the herein studied phenomena. In a recent study, Bastuji et al. (2020) recorded sleep spindles from different parts of the posterior thalamus. These results indicate that anterior, mediodorsal and posterior thalamic nuclei are involved in the proper functioning of the NREM sleep-related thalamo-cortical network, generating mid-frequency oscillations in the burst-firing mode.

In addition to detecting thalamic sleep spindles in human subjects, we revealed their association with thalamic ripples. SP (ripple) made up around 20% of overall ANT and MD sleep spindles, respectively. These spindles were of longer duration and characterized by different time-frequency activity profiles than sleep spindles in the absence of ripples: SP (ripple) was associated with an excess of thalamic ripple and larger spindle band (for both ANT and MD slow and fast spindles), and even theta band (for the ANT slow spindles) frequency activity compared to SP (pure). The increased ripple-band activity was the basis of ripples-associated sleep spindle definition. The spindle band activity occurred after about 500 ms from sleep spindle onset, which is assumed to reflect the elongation of ripple-associated sleep spindles.

The coordinated interactions between hippocampal ripples and cortical sleep spindles play a crucial role in memory formation (Latchoumane et al., 2017; Siapas & Wilson, 1998; Staresina et al., 2015). It was proposed that NREM sleep-based memory formation depends on the hierarchical nesting of slow waves, sleep spindles and hippocampal ripples, as these oscillations are instrumental in transferring information from the hippocampus to the neocortex (Diekelmann & Born, 2010; Staresina et al., 2015). In the past few years, accumulating evidence was found for the existence of ripples outside of the hippocampus (for a review, see McKenzie et al., 2020). Ripples were detected in several cortical areas, such as somatosensory and motor cortices (Averkin et al., 2016), olfactory cortices (Manabe et al., 2011), parahippocampal regions (Axmacher et al., 2008), and higher-order associational cortices as well (Khodagholy et al., 2017). These cortical ripples were frequently coupled with slower oscillations including sleep spindles. In the prefrontal cortex, mesio-temporal and neocortical structures, ripples were detected both before sleep spindles and locked to the spindle troughs (Bruder et al., 2021; Peyrache et al., 2011). Similar results were observed, confirming that cortical ripples were embedded into spindle troughs during natural sleep (Averkin et al., 2016). Although it is not entirely clear whether ripples in the thalamus are connected with pathological processes related to epilepsy. A close relationship between epilepsy and high-frequency oscillations (80–600 Hz, HFOs) occurrence is repeatedly found in animal and human studies (for a review, see Jiruska et al., 2017). In a recent study, Rektor et al. (2016) found HFOs in the human ANT up to 240 Hz frequency and 500 Hz frequency in one case, which was the first report of HFOs in the human thalamus. They suggested that these thalamic HFOs are related to pathological processes. In the current study, ripples (100–200 Hz) were described in both thalamic nuclei coupled with sleep spindles but also detected outside spindles during NREM sleep. We found a strong phase-amplitude coupling measured by the modulation index between the sleep spindle phase and ripple amplitude. This result suggests that in spite of the finding that ripples were as frequent during sleep spindles as during the whole NREM sleep (indicated by the lack of difference between ripple density/spindle minutes vs. ripple density/NREM minutes), spindle-associated ripples were strongly coupled to the sleep spindle oscillations both in the ANT and in the MD.

We found a positive correlation between the density of ripple-associated fast sleep spindles in the ANT and the Verbal Comprehension Index of our patients. This result suggests that ripples detected in the human ANT during NREM sleep may contribute to the preserved cognitive ability in the verbal domain. The cognitive functions of epilepsy patients have been extensively studied over the past few decades, but many questions remain

unclear. Memory dysfunctions, executive dysfunctions and decreased intelligence quotients are very common among epileptic patients, especially in terms of verbal ability, and vocabulary problems are also common in this population (Chakravarty et al., 2019). Indeed, the mean FSIQ was 76.23 (SD: 14.71) in our patients, which is well below the average range. Former studies reported that regardless of the anatomical location of the epileptic seizure focus, the patients had strongly reduced memory and executive function performance (Rai et al., 2015). Based on this result, it can be assumed that other causal factors play a role in the background of cognitive decline. There are only a few such studies in the literature that comprehensively investigate the role of different clinical and polysomnographic sleep parameters in the cognitive functions of epilepsy patients (see, however, Chakravarty et al., 2019; Schiller et al., 2022). In the study of Schiller et al. (2022), reduced fast spindle density was measured for epilepsy patients, and the local reduction of fast spindles negatively correlated with attentional task performance. Kramer et al. (Kramer et al., 2021) found a positive relationship between sleep spindle density and general intelligence measured by FSIQ in children with focal epilepsy. They suggested that the dysfunction of the thalamocortical system also impairs the generation of sleep spindles, which play an essential role in memory functions. Our results show that fast sleep spindles associated with ripples in the thalamus may play a role in preserved verbal functioning, as measured by the Verbal Comprehension Index. Note, however, that there are particular limitations of the analysis: the sample size is small and the FSIQ and index scores are below the average of our patients, and even though we used strict corrections to avoid Type I errors, a larger number of samples and replications would be necessary.

The temporal dynamics of sleep spindles in the thalamus and the scalp show that cortical spindles preceded thalamic spindles, especially those associated with ripples. Sleep spindles are generated by the reticular thalamic nucleus and propagate to the cortex through thalamo-cortical network (Steriade, 2005; Steriade et al., 1987). The temporal advantage of the scalp sleep spindles suggests that ANT and MD sleep spindles are propagated through cortico-thalamic networks and not directly through thalamo-thalamic projections. It was suggested that cortico-thalamic feedback projections from the cortical sites to the reticular thalamus are responsible for the large-scale synchronization of sleep spindles (Destexhe et al., 1998). The ANT has a bidirectional connection with the anterior cingulate cortex, retrosplenial cortex and subiculum, whereas the MD is interconnected with the medial-prefrontal cortex (Aggleton et al., 2010; Mitchell & Chakraborty, 2013; Pergola et al., 2018). The recent results suggest that sleep spindles propagate through these cortical sites to the ANT and MD. Thus, the thalamus seems to play an important interface between the propagation of these neural oscillations in the hippocampal-prefrontal network.

Former studies suggested that the human ANT contributes to the epileptic network, and the ANT became an important target for DBS in epilepsy treatment (Hodaie et al., 2002; Salanova, 2018; Sweeney-Reed et al., 2016). Furthermore, interictal discharges were also detected in the MD (Sweeney-Reed et al., 2016). Although there is no direct anatomical connection between the ANT and MD, this report indicates that the MD might be involved in the epileptic circuitry as well. Our current results further support this assumption. However, we did not find a significant correlation between sleep spindle density and clinical epilepsy characteristics; the presence of different sleep spindles (slow vs fast) could be also indicative of specific network dysfunctions besides interictal discharges. Sleep spindles in the mediodorsal thalamus were also indicative in schizophrenia patients, where a negative association was found between the volume of the MD and scalp-recorded sleep spindle density (Ferrarelli & Tononi, 2017). Thus, the MD can be a new, potential target for future research. The current results support the involvement of the human thalamus in sleep spindle-related neural activity. Sleep spindles were found in the ANT and in the MD, and ripples coupled with sleep spindles resulted in distinguishable spectro-temporal differences in the thalamus but not at the scalp. The major finding is that ripples are also present in the thalamus, which seems to contribute to intellectual ability through a tight interaction between spindles and ripples. The limitations of the study are no direct testing of offline memory processes during sleep. Co-registration from the hippocampus, thalamus and scalp will present an opportunity to reveal the hippocampal-thalamo-cortical pathway in further research, providing target circuits for neuromodulation and therapeutics. Furthermore, our participants suffered from medically refractory epilepsy being subjects of poly-antiseizure medication treatment. This type of treatment was shown to reduce sleep slow wave (0.1–2 Hz) EEG amplitude, increase sleep spindle frequency (11–16 Hz) power and decrease slow wave-sleep spindle cross-frequency coupling in epilepsy patients (Roebber et al., 2022). Moreover, sleep might be fragmented especially in the few days after the operation (Lendner & Helfrich, 2023). As our present investigation focuses on sleep spindle-related activity of epilepsy patients we cannot entirely exclude the possibility that our reported findings are indeed partially influenced by antiseizure medications. Further investigations focusing on the

thalamic recordings of patient groups with different medications are needed in order to provide unequivocal evidence for the claims we made in our paper.

AUTHOR CONTRIBUTIONS

O.S. and R.B. designed research; O.S., P.S., P.P.U., Z.J., L.H., L.E., D.F. and R.B. performed research; O.S., P.S., P.P.U., Z.J., L.H., L.E., D.F. and R.B. analyzed data; O.S., P.P.U. and R.B. wrote the paper.

ACKNOWLEDGEMENTS

The work was supported by the National Research, Development and Innovation Office of Hungary Grant NKFI_FK_128100, K_128117, the ELTE Thematic Excellence Program 2020 TKP2020-IKA-05, and the Ministry of Innovation and Technology of Hungary from the National Research, Development and Innovation Fund, financed under the TKP2021-EGA-25 funding scheme.

CONFLICT OF INTEREST STATEMENT

The authors declare no competing conflict of interest.

PEER REVIEW

The peer review history for this article is available at https://www.webofscience.com/api/gateway/wos/peer-review/10.1111/ejn.16240.

DATA AVAILABILITY STATEMENT

Whole night thalamic LFP data are available here: https://osf.io/q2yph/, https://osf.io/bz4na/, https://osf.io/temya/, https://osf.io/p8dqb/, https://osf.io/852j4/

REFERENCES

Aggleton, J. P., O'Mara, S. M., Vann, S. D., Wright, N. F., Tsanov, M., & Erichsen, J. T. (2010). Hippocampal-anterior thalamic pathways for memory: Uncovering a network of direct and indirect actions. *European Journal of Neuroscience*, *31*(12), 2292–2307. https://doi.org/10.1111/j.1460-9568.2010.07251.x

Averkin, R. G., Szemenyei, V., Bordé, S., & Tamás, G. (2016). Identified cellular correlates of neocortical ripple and high-gamma oscillations during spindles of natural sleep. *Neuron*, *92*(4), 916–928. https://doi.org/10.1016/j.neuron.2016.09.032

Axmacher, N., Elger, C. E., & Fell, J. (2008). Ripples in the medial temporal lobe are relevant for human memory consolidation. *Brain: a Journal of Neurology*, *131*(7), 1806–1817. https://doi.org/10.1093/brain/awn103

Bastuji, H., Lamouroux, P., Villalba, M., Magnin, M., & Garcia-Larrea, L. (2020). Local sleep spindles in the human thalamus. *The Journal of Physiology*, *598*(11), 2109–2124. https://doi.org/10.1113/JP279045

Berry, R. B., R. Brooks, C. E. Gamaldo, S. M. Harding, R. M. Lloyd, C. L. Marcus, and B. V. Vaughn. 2015. *AASM|scoring manual version 2.2 the AASM manual for the scoring of sleep and associated events RULES, TERMINOLOGY AND TECHNICAL SPECIFICATIONS VERSION 2.2*. Darien, IL: American Academy of Sleep.

Bódizs, R., Kis, T., Lázár, A. S., Havrán, L., Rigó, P., Clemens, Z., & Halász, P. (2005). Prediction of general mental ability based on neural oscillation measures of sleep. *Journal of Sleep Research*, *14*(3), 285–292. https://doi.org/10.1111/j.1365-2869.2005.00472.x

Bódizs, R., Körmendi, J., Rigó, P., & Lázár, A. S. (2009). The individual adjustment method of sleep spindle analysis: Methodological improvements and roots in the fingerprint paradigm. *Journal of Neuroscience Methods*, *178*(1), 205–213. https://doi.org/10.1016/j.jneumeth.2008.11.006

Bruder, J. C., Schmelzeisen, C., Lachner-Piza, D., Reinacher, P., Schulze-Bonhage, A., & Jacobs, J. (2021). Physiological ripples associated with sleep spindles can be identified in patients with refractory epilepsy beyond Mesio-temporal structures. *Frontiers in Neurology*, *12*, 612293. https://doi.org/10.3389/fneur.2021.612293

Buchmann, A., Dentico, D., Peterson, M. J., Riedner, B. A., Sarasso, S., Massimini, M., Tononi, G., & Ferrarelli, F. (2014). Reduced Mediodorsal thalamic volume and prefrontal cortical spindle activity in schizophrenia. *NeuroImage*, *102*(P2), 540–547. https://doi.org/10.1016/j.neuroimage.2014.08.017

Cairney, S. A., Guttesen, A. V., Marj, N. E., & Staresina, B. P. (2018). Memory consolidation is linked to spindle-mediated information processing during sleep. *Current Biology*, *28*(6), 948–954.e4. https://doi.org/10.1016/j.cub.2018.01.087

Chakravarty, K., Shukla, G., Poornima, S., Agarwal, P., Gupta, A., Mohammed, A., Ray, S., Pandey, R. M., Goyal, V., Srivastava, A., & Behari, M. (2019). Effect of sleep quality on memory, executive function, and language performance in patients with refractory focal epilepsy and controlled epilepsy versus healthy controls – A prospective study. *Epilepsy and Behavior*, *92*, 176–183. https://doi.org/10.1016/j.yebeh.2018.12.028

Chatburn, A., Coussens, S., Lushington, K., Kennedy, D., Baumert, M., & Kohler, M. (2013). Sleep spindle activity and cognitive performance in healthy children. *Sleep*, *36*(2), 237–243. https://doi.org/10.5665/sleep.2380

Clemens, Z., Mölle, M., Erőss, L., Jakus, R., Rásonyi, G., Halász, P., & Born, J. (2011). Fine-tuned coupling between human Parahippocampal ripples and sleep spindles. *European Journal of Neuroscience*, *33*(3), 511–520. https://doi.org/10.1111/j.1460-9568.2010.07505.x

Destexhe, A., Contreras, D., & Steriade, M. (1998). Mechanisms underlying the synchronizing action of Corticothalamic feedback through inhibition of thalamic relay cells. *Journal of Neurophysiology*, *79*(2), 999–1016. https://doi.org/10.1152/jn.1998.79.2.999

Deutschová, B., Klimeš, P., Jordan, Z., Jurák, P., Erőss, L., Lamoš, M., Halámek, J., Daniel, P., Rektor, I., & Fabo, D. (2021). Thalamic oscillatory activity may predict response to deep brain stimulation of the anterior nuclei of the thalamus. *Epilepsia*, *62*(5), e70–e75. https://doi.org/10.1111/epi.16883

Diekelmann, S., & Born, J. (2010). The memory function of sleep. *Nature Reviews Neuroscience*, *11*(2), 114–126. https://doi.org/10.1038/nrn2762

Fama, R., & Sullivan, E. V. (2015). Thalamic structures and associated cognitive functions: Relations with age and aging. *Neuroscience and Biobehavioral Reviews*, *54*, 29–37. https://doi.org/10.1016/j.neubiorev.2015.03.008

Ferrarelli, F., & Tononi, G. (2017). Reduced sleep spindle activity point to a TRN-MD thalamus-PFC circuit dysfunction in schizophrenia. *Schizophrenia Research*, *180*, 36–43. https://doi.org/10.1016/j.schres.2016.05.023

Fogel, S. M., & Smith, C. T. (2011). The function of the sleep spindle: A physiological index of intelligence and a mechanism for sleep-dependent memory consolidation. *Neuroscience and Biobehavioral Reviews*, *35*(5), 1154–1165. https://doi.org/10.1016/j.neubiorev.2010.12.003

Gelinas, J. N., Khodagholy, D., Thesen, T., Devinsky, O., & Buzsáki, G. (2016). Interictal epileptiform discharges induce hippocampal-cortical coupling in temporal lobe epilepsy. *Nature Medicine*, *22*(6), 641–648. https://doi.org/10.1038/nm.4084

Girardeau, G., & Zugaro, M. (2011). Hippocampal ripples and memory consolidation. *Current Opinion in Neurobiology*, *21*(3), 452–459. https://doi.org/10.1016/j.conb.2011.02.005

Halász, P., Bódizs, R., Ujma, P. P., Fabó, D., & Szűcs, A. (2019). Strong relationship between NREM sleep, epilepsy and plastic functions — A conceptual review on the neurophysiology background. *Epilepsy Research*, *150*, 95–105. https://doi.org/10.1016/j.eplepsyres.2018.11.008

Halász, P., & Szűcs, A. (2020). Sleep and epilepsy link by plasticity. *Frontiers in Neurology*, *11*, 911. https://doi.org/10.3389/fneur.2020.00911

Hodaie, M., Wennberg, R. A., Dostrovsky, J. O., & Lozano, A. M. (2002). Chronic anterior thalamus stimulation for intractable epilepsy. *Epilepsia*, *43*(6), 603–608. https://doi.org/10.1046/j.1528-1157.2002.26001.x

Huguenard, J. R., & McCormick, D. A. (2007). Thalamic synchrony and dynamic regulation of global forebrain oscillations. *Trends in Neurosciences*, *30*(7), 350–356. https://doi.org/10.1016/j.tins.2007.05.007

Jasper, H. H. (1958). The ten-twenty electrode system of the international federation. *Electroencephalography and Clinical Neurophysiology*, *10*, 371–375.

Jiruska, P., Alvarado-Rojas, C., Schevon, C. A., Staba, R., Stacey, W., Wendling, F., & Avoli, M. (2017). Update on the mechanisms and roles of high-frequency oscillations in seizures and epileptic disorders. *Epilepsia*, *58*(8), 1330–1339. https://doi.org/10.1111/epi.13830

Khodagholy, D., Gelinas, J. N., & Buzsáki, G. (2017). Learning-enhanced coupling between ripple oscillations in association cortices and hippocampus. *Science (New York, N.Y.)*, *358*(6361), 369–372.

Kramer, M. A., Stoyell, S. M., Chinappen, D., Ostrowski, L. M., Spencer, E. R., Morgan, A. K., Emerton, B. C., Jing, J., Westover, M. B., Eden, U. T., Stickgold, R., Manoach, D. S., & Chu, C. J. (2021). Focal sleep spindle deficits reveal focal Thalamocortical dysfunction and predict cognitive deficits in sleep activated developmental epilepsy. *Journal of Neuroscience*, *41*(8), 1816–1829. https://doi.org/10.1523/JNEUROSCI.2009-20.2020

Latchoumane, C. F. V., Ngo, H. V. V., Born, J., & Shin, H. S. (2017). Thalamic spindles promote memory formation during sleep through triple phase-locking of cortical, thalamic, and hippocampal rhythms. *Neuron*, *95*(2), 424–435.e6. https://doi.org/10.1016/j.neuron.2017.06.025

Lendner, J. D., & Helfrich, R. F. (2023). How Can I Run Sleep and Anesthesia Studies with Intracranial EEG? In N. Axmacher (Ed.), *Intracranial EEG. Studies in neuroscience, psychology and behavioral economics*. Springer. https://doi.org/10.1007/978-3-031-20910-9_20

Mak-Mccully, R. A., Rolland, M., Sargsyan, A., Gonzalez, C., Magnin, M., Chauvel, P., Rey, M., Bastuji, H., & Halgren, E. (2017). Coordination of cortical and thalamic activity during non-REM sleep in humans. *Nature Communications*, *8*(1), 15499. https://doi.org/10.1038/ncomms15499

Manabe, H., Kusumoto-Yoshida, I., Ota, M., & Mori, K. (2011). Olfactory cortex generates synchronized top-down inputs to the olfactory bulb during slow-wave sleep. *The Journal of Neuroscience*, *31*(22), 8123–8133. https://doi.org/10.1523/JNEUROSCI.6578-10.2011

Manzano, G. M., Ragazzo, P. C., Tavares, S. M., & Marino, R. Jr. (1986). Anterior zygomatic electrodes: A special electrode for the study of temporal lobe epilepsy. *Stereotactic and Functional Neurosurgery*, *49*(4), 213–217. https://doi.org/10.1159/000100148

Maris, E., & Oostenveld, R. (2007). Nonparametric statistical testing of EEG- and MEG-data. *Journal of Neuroscience Methods*, *164*(1), 177–190. https://doi.org/10.1016/j.jneumeth.2007.03.024

McKenzie, S., Nitzan, N., & English, D. F. (2020). Mechanisms of neural organization and rhythmogenesis during hippocampal and cortical ripples. *Philosophical Transactions of the Royal Society B*, *375*(1799), 20190237. https://doi.org/10.1098/rstb.2019.0237

Mitchell, A. S., & Chakraborty, S. (2013). What does the Mediodorsal thalamus do? *Frontiers in Systems Neuroscience*, *7*(37), 37. https://doi.org/10.3389/fnsys.2013.00037

Pergola, G., Danet, L., Pitel, A. L., Carlesimo, G. A., Segobin, S., Pariente, J., Suchan, B., Mitchell, A. S., & Barbeau, E. J. (2018). The regulatory role of the human Mediodorsal thalamus. *Trends in Cognitive Sciences*, *22*(11), 1011–1025. https://doi.org/10.1016/j.tics.2018.08.006

Peyrache, A., Battaglia, F. P., & Destexhe, A. (2011). Inhibition recruitment in prefrontal cortex during sleep spindles and gating of hippocampal inputs. *Proceedings of the National Academy of Sciences of the United States of America*, *108*(41), 17207–17212. https://doi.org/10.1073/pnas.1103612108

Rai, V. K., Shukla, G., Afsar, M., Poornima, S., Pandey, R. M., Rai, N., Goyal, V., Srivastava, A., Vibha, D., & Behari, M. (2015). Memory, executive function and language function are similarly impaired in both temporal and extra temporal refractory epilepsy—A prospective study. *Epilepsy Research*, *109*(1), 72–80. https://doi.org/10.1016/j.eplepsyres.2014.09.031

Rektor, I., Doležalová, I., Chrastina, J., Jurák, P., Halámek, J., Baláž, M., & Brázdil, M. (2016). High-frequency oscillations in the human anterior nucleus of the thalamus. *Brain Stimulation*, *9*(4), 629–631. https://doi.org/10.1016/j.brs.2016.04.010

Roebber, J. K., Lewis, P. A., Crunelli, V., Navarrete, M., & Hamandi, K. (2022). Effects of anti-seizure medication on sleep spindles and slow waves in drug-resistant epilepsy. *Brain*

Sciences, *12*(10), 1288. https://doi.org/10.3390/brainsci12101288

Salanova, V. (2018). Deep brain stimulation for epilepsy. *Epilepsy and Behavior*, *88*, 21–24. https://doi.org/10.1016/j.yebeh.2018.06.041

Saletin, J. M., Goldstein, A. N., & Walker, M. P. (2011). The role of sleep in directed forgetting and remembering of human memories. *Cerebral Cortex*, *21*(11), 2534–2541. https://doi.org/10.1093/cercor/bhr034

Schiller, K., Avigdor, T., Abdallah, C., Sziklas, V., Crane, J., Stefani, A., Peter-Derex, L., & Frauscher, B. (2022). Focal epilepsy disrupts spindle structure and function. *Scientific Reports*, *12*(1), 11137. https://doi.org/10.1038/s41598-022-15147-0

Siapas, A. G., & Wilson, M. A. (1998). Coordinated interactions between hippocampal ripples and cortical spindles during slow-wave sleep. *Neuron*, *21*(5), 1123–1128. https://doi.org/10.1016/S0896-6273(00)80629-7

Simor, P., Szalárdy, O., Gombos, F., Ujma, P. P., Jordán, Z., Halász, L., Erőss, L., Fabó, D., & Bódizs, R. (2021). REM sleep microstates in the human anterior thalamus. *The Journal of Neuroscience* JN-RM-1899-20, *41*, 5677–5686. https://doi.org/10.1523/JNEUROSCI.1899-20.2021

Staresina, B. P., Bergmann, T. O., Bonnefond, M., Van Der Meij, R., Jensen, O., Deuker, L., Elger, C. E., Axmacher, N., & Fell, J. (2015). Hierarchical nesting of slow oscillations, spindles and ripples in the human hippocampus during sleep. *Nature Neuroscience*, *18*(11), 1679–1686. https://doi.org/10.1038/nn.4119

Steriade, M. (2005). Sleep, epilepsy and thalamic reticular inhibitory neurons. *Trends in Neurosciences*, *28*(6), 317–324. https://doi.org/10.1016/j.tins.2005.03.007

Steriade, M., Domich, L., Oakson, G., & Deschenes, M. (1987). The Deafferented reticular thalamic Nucleas generates spindle rhythmicity. *Journal of Neurophysiology*, *57*(1), 260–273. https://doi.org/10.1152/jn.1987.57.1.260

Sweeney-Reed, C. M., Lee, H., Rampp, S., Zaehle, T., Buentjen, L., Voges, J., Holtkamp, M., Hinrichs, H., Heinze, H. J., & Schmitt, F. C. (2016). Thalamic Interictal epileptiform discharges in deep brain stimulated epilepsy patients. *Journal of Neurology*, *263*(10), 2120–2126. https://doi.org/10.1007/s00415-016-8246-5

Tort, A. B. L., Komorowski, R., Eichenbaum, H., & Kopell, N. (2010). Measuring phase-amplitude coupling between neuronal oscillations of different frequencies. *Journal of Neurophysiology*, *104*(2), 1195–1210. https://doi.org/10.1152/jn.00106.2010

Tsai, Y. T., Chan, H. L., Lee, S. T., Tu, P. H., Chang, B. L., & Wu, T. (2010). Significant Thalamocortical coherence of sleep spindle, theta, Delta, and slow oscillations in NREM sleep: Recordings from the human thalamus. *Neuroscience Letters*, *485*(3), 173–177. https://doi.org/10.1016/j.neulet.2010.09.004

Ujma, P. P. (2018). Sleep spindles and general cognitive ability – A meta-analysis. *Sleep Spindles & Cortical up States*, *1*, 1–17.

Ujma, P. P., Bódizs, R., & Dresler, M. (2020). Sleep and intelligence: Critical review and future directions. *Current Opinion in Behavioral Sciences*, *33*, 109–117. https://doi.org/10.1016/j.cobeha.2020.01.009

Ujma, P. P., Gombos, F., Genzel, L., Konrad, B. N., Simor, P., Steiger, A., Dresler, M., & Bódizs, R. (2015). A comparison of two sleep spindle detection methods based on all night averages: Individually adjusted vs. fixed frequencies. *Frontiers in Human Neuroscience*, *9*, 52. https://doi.org/10.3389/fnhum.2015.00415

Ujma, P. P., Szalárdy, O., Fabó, D., Erőss, L., & Bódizs, R. (2022). Thalamic activity during scalp slow waves in humans. *NeuroImage*, *257*, 119325. https://doi.org/10.1016/j.neuroimage.2022.119325

Wechsler, D. (2008). *Wechsler adult intelligence scale—Fourth edition administration and scoring manual*. Pearson.

Wilson, M. A., & McNaughton, B. L. (1994). Reactivation of hippocampal ensemble memories during sleep. *Science*, *265*(5172), 676–679. https://doi.org/10.1126/science.8036517

Wolff, M., Morceau, S., Folkard, R., Martin-Cortecero, J., & Groh, A. (2021). A thalamic Bridge from sensory perception to cognition. *Neuroscience & Biobehavioral Reviews*, *120*, 222–235. https://doi.org/10.1016/j.neubiorev.2020.11.013

SUPPORTING INFORMATION

Additional supporting information can be found online in the Supporting Information section at the end of this article.

How to cite this article: Szalárdy, O., Simor, P., Ujma, P. P., Jordán, Z., Halász, L., Erőss, L., Fabó, D., & Bódizs, R. (2024). Temporal association between sleep spindles and ripples in the human anterior and mediodorsal thalamus. *European Journal of Neuroscience*, *59*(4), 641–661. https://doi.org/10.1111/ejn.16240